Materials Characterization 132 (2017) 381–387

Contents lists available at ScienceDirect

Materials Characterization

journal homepage: www.elsevier.com/locate/matchar

Microstructural characterizations on Mn-containing intermetallic phases in a high-pressure die-casting Mg–4Al–4RE–0.3Mn alloy

Qiang Yang[a], Kai Guan[a,d], Baishun Li[a,d], Shuhui Lv[b], Fanzhi Meng[b,*], Wei Sun[a], Yaqin Zhang[c], Xiaojuan Liu[a], Jian Meng[a,*]

[a] State Key Laboratory of Rare Earth Resource Utilization, Changchun Institute of Applied Chemistry, Chinese Academy of Sciences, Changchun 130022, PR China
[b] School of Materials Science and Engineering, Changchun University of Science and Technology, 130022, PR China
[c] Kashui International Holdings Limited, Shenzhen, Guangdong 518111, PR China
[d] University of Sciences & Technology of China, Hefei 230026, PR China

ARTICLE INFO

Keywords:
Transmission electron microscopy (TEM)
Magnesium alloys
Die-casting
Al-Mn intermetallic phase
Twins

ABSTRACT

The types and the detailed structures of the Mn-containing phases in the high-pressure die-casting Mg–4Al–4RE–0.3Mn alloy were thoroughly investigated using transmission electron microscopy (TEM). The results reveal five Mn-containing intermetallic phases with different morphologies, namely the regular blocky phase, the irregular blocky phase, the interlaced lath-shaped phase, the nano-scale phase on the surface of or embedded in the $Al_{11}RE_3$ particles, and the nano-scale precipitate in the α-Mg matrix. The former twos belong to $Al_{10}RE_2Mn_5$ but the latter one contains numerous normal (11.1) twins and orientation twins. In addition, the third one simultaneously contains $Al_{10}RE_2Mn_5$ and Al_8REMn_4, of which both are coherent with each other and contain normal twins. Finally, the last two nano-scale Mn-containing phases on the surface of or embedded in $Al_{11}RE_3$ and precipitated in α-Mg grains are $Al_{10}RE_2Mn_7$ and Al_8Mn_5, respectively.

1. Introduction

High-pressure die-casting (HPDC) Mg–Al–RE-based alloys are growingly attractive in applying to power-train components in automobile and aerospace industries due to their outstanding high-temperature mechanical properties and creep resistance [1–3]. Ordinarily, manganese primarily considered as an iron remover is added into Mg–Al–RE-based alloys to improve their corrosion resistance [4,5]. As a result, some Mn-containing intermetallic phases either formed during solidification or during following heat treatments will inevitably remain in the alloys. For instance, Pettersell et al. [6] reported that there is only one Mn-containing intermetallic phase with a lumpy form and sizes of 0.5–4 μm in a die-casting Mg–4Al–1.4RE–0.4Mn alloy, which was identified as $Al_{10}RE_2Mn_7$ (rhombohedral structure, $a = 0.904$ nm and $c = 1.317$ nm). Afterwards, $Al_{10}RE_2Mn_7$ phase was widely reported in various Mg–Al–RE-based alloys, with hexagonal, lumpy or rectangular shape and sizes in the range of 0.2–20 μm [7–15]. However, scarce investigators paid attention to the structural differences among the $Al_{10}RE_2Mn_7$ particles with different morphologies. Then, Yang et al. [16] reported a new nano-scale Mn-containing particle (8–45 nm) located on the surface of $Al_{11}RE_3$ particles in a die-casting Mg–4Al–4-La–0.4Mn alloy, but its crystal structure was not confirmed although with a high-resolution transmission electron microscopy (HR-TEM) image. Recently, Zhu et al. [9,10] also reported a new nano-scale Mn-containing intermetallic particle precipitated during artificial aging or creep and it can significantly improve both strengths and creep resistance of the Mn-containing die-casting Mg–4Al–3La alloys. Unfortunately, the crystal structure of the Mn-containing precipitate was also not revealed based on HR-TEM images in their work. With respect to the conventional AZ31 (Mg–3Al–1Zn) alloy, several Al-Mn intermetallics such as Al_4Mn, $Al_{11}Mn_5$ and Al_8Mn_5 were predicted when Mn is added by Stanford et al. [17], and then monitored by Dogan et al. [18] when studying the dynamic precipitation in a Mn-containing AZ31 alloy during different plastic deformation modes. In addition, Pan et al. [19] also investigated the types and distribution characterization of the Al-Mn phases in the conventional Mg–6Al–1Zn based alloy. However, there is still no open literature conclusively revealing the types and the corresponding detailed structures of the Mn-containing intermetallic particles in the Mg–Al–RE based alloys to date, which results in a limited understanding of their formation mechanisms, much less how to control the phase and the morphology.

To well understanding the formation mechanisms and provide theoretical support on how to control the phase and the morphology of the Mn-containing intermetallic particles formed in die-casting

---

* Corresponding authors.
E-mail addresses: mengfanzhi@cust.edu.cn (F. Meng), jmeng@ciac.ac.cn (J. Meng).

http://dx.doi.org/10.1016/j.matchar.2017.08.032
Received 8 August 2017; Received in revised form 24 August 2017; Accepted 24 August 2017

Mg–Al–RE based alloys, it is significantly important to systematically investigate the types and the detailed microstructures of the Mn-containing intermetallic particles with various morphologies. In this paper, a die-casting Mg–4Al–4RE–0.3Mn (ARE44, RE = Ce and La) alloy was selected and various Mn-containing intermetallic phases were thoroughly investigated, and the detailed structural characteristics plus crystallographic orientation information in different particles were revealed using transmission electron microscopy (TEM).

2. Experimental Material and Procedures

The studied ARE44 alloy was prepared from high-purity magnesium, pure aluminum, Mg–20 wt% CeLa, and Mg–2 wt% Mn master alloys. The melt was firstly produced in a resistance heated crucible under the protection of continuously flushed CO_2 + 1 vol% SF_6 mixed gas, and then casted using a 280 ton clamping force cold chamber die-cast machine. Finally, its chemical compositions were determined by inductivity coupled plasma atomic emission spectroscopy (ICP-AES) apparatus, and are Mg–3.73Al–1.97Ce–1.76La–0.27Mn in mass%. In addition, a heat treatment (at 350 °C for 16 h followed by cool water quenching) which can avoid the precipitation of $Mg_{17}Al_{12}$, were conducted on a part of the specimens. Microstructural analysis was conducted using a FEI Tecnai G20 TEM with an accelerating voltage of 200 kV and equipped with an energy dispersive spectrometer (EDS). TEM foils in the form of 3 mm diameter discs were mechanically grounded to approximately 30 μm and then ion-milled by a precision ion polishing system (PIPS Gatan) equipped with cooling system by liquid nitrogen.

3. Results and Discussion

Fig. 1a–c shows the bright-field TEM image, the corresponding selected area electron diffraction (SAED) pattern and HR-TEM image of a typical blocky Mn-containing particle with relatively regular outlines. The results indicate that the regular blocky phase is $Al_{10}RE_2Mn_5$ phase, with no obvious twins or other substructures. However, the regular blocky $Al_{10}RE_2Mn_5$ phase was relatively less frequently observed in the studied alloy, compared with another one Mn-containing phase with irregular outlines, whose representative bright-field TEM image along with the corresponding selected area electron diffraction (SAED) pattern and the corresponding HR-TEM image were shown in Fig. 1d–f, respectively. It can be seen that the irregular blocky Mn-containing phase is still $Al_{10}RE_2Mn_5$ phase. However, it simultaneously contains several parts with different orientations and also some (11.1) twins can be observed in a certain part. Furthermore, the HR-TEM image (Fig. 1f) also indicates that there are some dislocations associated with the twin boundary (TB), but with no stacking faults. It is reported that when an extended dislocation recombines or constricts into a perfect dislocation configuration at the coherent TB, it will slip through the boundary by splitting into three Shockley partials, finally formed a step [20]. Since no tacking faults were observed in the irregular blocky $Al_{10}RE_2Mn_5$ phase, the TB steps would probably form by some other mechanisms. In addition, the TBs with dislocation-TB interactions in the $Al_{10}RE_2Mn_5$ phase afford more room for storage of dislocations, which might be conductive to increasing strain hardening of the alloys [21].

Fig. 2a also shows a representative bright-field TEM graph of an irregular blocky $Al_{10}RE_2Mn_5$ phase, with the corresponding SAED patterns from its part B and part C shown in Fig. 2b and c, respectively. It further indicates that the several parts in the irregular $Al_{10}RE_2Mn_5$ phase are relatively independent, with no obvious orientation relationship between them. Additionally, it can also be seen from Fig. 2c that there some extra diffraction contrast spots except those from the twinned $Al_{10}RE_2Mn_5$ domains with **B** = $[1\bar{5}.3]$. According to the intensity diagrams along the purple (the left inset in Fig. 2c) and the red (the right inset in Fig. 2c) dotted lines, the extra diffraction contrast spots correspond to the main interplanar spacing of two perpendicular

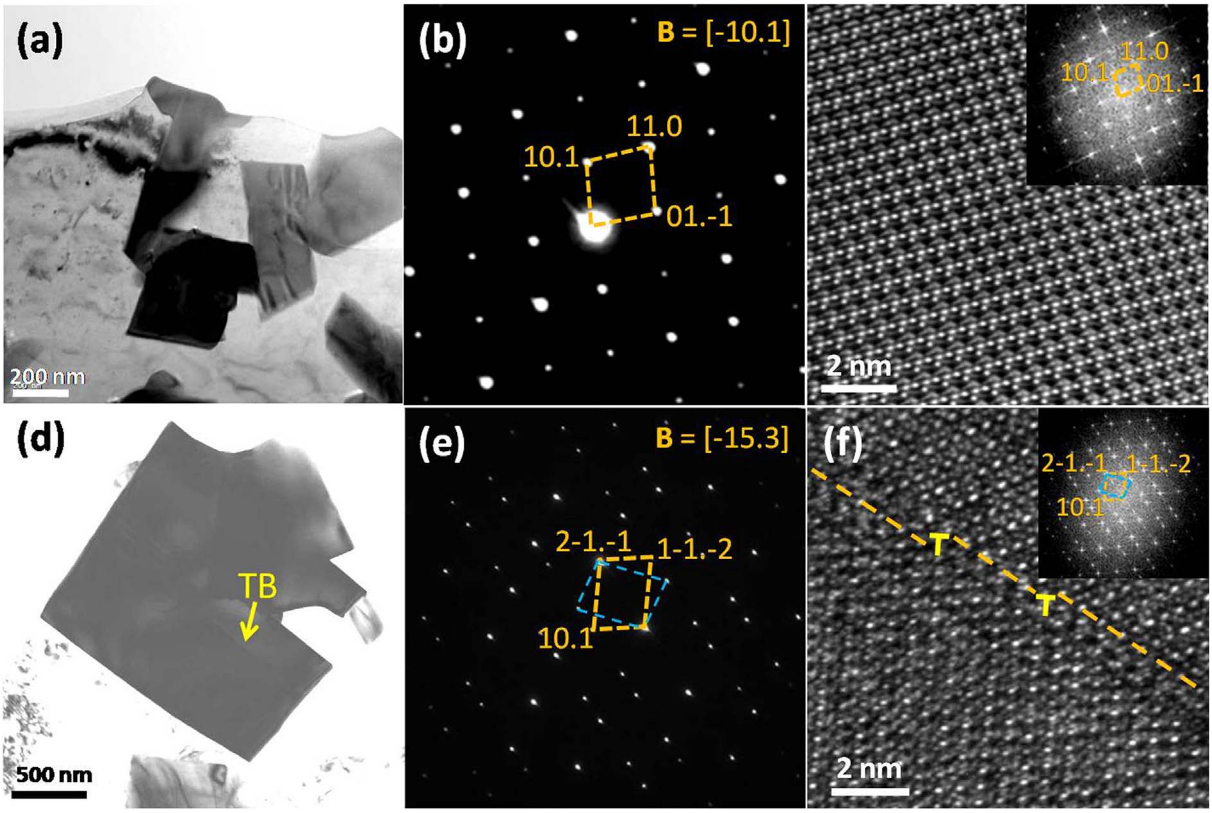

Fig. 1. (a, d) Bright-field TEM images, (b, e) the corresponding SAED patterns, and (c, f) the corresponding HR-TEM images along with the FFT patterns for the regular blocky phase and the irregular blocky phase, respectively.